Available online at www.sciencedirect.com

ScienceDirect

Journal of Hydro-environment Research 12 (2016) 59–69

Journal of Hydro-environment Research

www.elsevier.com/locate/jher

Research papers

Bulk drag of a regular array of emergent blade-type vegetation stems under gradually varied flow

A.O. Busari, C.W. Li *

Department of Civil and Environmental Engineering, The Hong Kong Polytechnic University, HKSAR, China

Received 26 June 2015; revised 30 December 2015; accepted 19 February 2016

Available online 16 March 2016

Abstract

The drag induced by flow through vegetation is affected by the velocity, shape of vegetation stems and wake interference among stems. To account for the interference effects, previous works generally related the bulk drag coefficient of vegetation to the solid volume fraction ϕ of the vegetated zone, and the trends of the results were found to be inconsistent. In this work, a systematic laboratory study has been carried out to investigate the effect of the distribution pattern of vegetation stems on the hydrodynamics of gradually varied flow through emergent blade-type vegetation. The finite artificial vegetation patches of solid volume fractions ranging from 0.005 to 0.121 have been used and the stem Reynolds number ranges from 500–2600. The longitudinal water surface profiles have been measured, and the effect of increasing roughness density with respect to varying longitudinal and lateral spacing under the flow conditions is examined. The momentum equation that relates the vegetation resistant force and water surface profile has been used to obtain the mean bulk drag coefficient C_d of the canopy. The results show that C_d decreases with increasing stem Reynolds number, decreases with increasing ϕ at fixed lateral spacing due to sheltering effect, and increases with ϕ at fixed longitudinal spacing due to channeling effect. An empirical equation has been obtained relating C_d to the lateral and longitudinal spacing instead of ϕ.

Keywords: Drag coefficient; Interference effects; Emergent vegetation; Gradually varied flow

1. Introduction

Vegetation occurs in riverine environment and is commonly found along the banks, in channel or on the floodplain. It has a significant influence on the behavior of the fluvial system. The benefits rendered by vegetation such as storm surge protection, providing habitat for aquatic animals, bank/channel stabilization and water quality improvement motivate the research of vegetated flows. For river and coastal management, the planting of vegetation along channels and coastal areas increases the hydraulic resistance, reduces flow speed and hence erosion. The increasing hydraulic resistance is due to the viscous and pressure drags on the plants. The pressure drag is dominating and proportional to the square of the velocity, with the constant of proportion called the drag coefficient. The vegetation induced drag and the associated drag coefficient depends on the properties of vegetation, such as areal density, flexibility, patchiness, age, seasonality, and foliage (e.g., Li and Xie, 2011, Nikora et al., 2008, Stone and Shen, 2002; Tanino and Nepf, 2008, Wu et al., 1999, Yang and Choi, 2009, Zeng and Li, 2014). The mean drag coefficient of a vegetation zone is then called the bulk drag coefficient C_d (e.g., Nepf, 1999). In the simulation of vegetated flows, C_d is an important input parameter to the theoretical, (semi)empirical or numerical model and its accurate estimation is essential (Busari and Li, 2014).

The fact that the areal density of vegetation will affect the drag coefficient has been recognized in previous studies, including Fathi-Moghadam and Kouwen (1997), Nepf (1999), Armanini et al. (2005), James et al. (2004), Righetti and Armanini (2002), Kouwen and Fathi-Moghadam (2000). Various studies suggested there are different trends for the bulk drag coefficient against areal density of vegetation (λ) for cylinder arrays. Nepf (1999) developed a wake interference model to account for the reduction of drag coefficient of a cylinder in an array. The model predicts that the bulk drag coefficient

* Corresponding author. C.W. Li, Department of Civil and Environmental Engineering, The Hong Kong Polytechnic University, HKSAR, China. Tel.: +852 27666043; fax: +852 23346389.

E-mail address: cecwli@polyu.edu.hk (C.W. Li).

http://dx.doi.org/10.1016/j.jher.2016.02.003

1570-6443/

decreases with the increase in solid volume fraction ϕ. The model results were supported by some available experimental data (Kays and London, 1955; Zdravkovich, 1993).

On the contrary, Stone and Shen (2002) found that the bulk drag coefficient increases with the solid volume fraction for an array of cylinders with staggered arrangement. The use of the velocity between the stems as the velocity scale reduces the bulk drag coefficient, which becomes closer to that of an isolated cylinder. Tanino and Nepf (2008) carried out experiments to determine drag in a random array of cylinders and found that the bulk drag coefficient increases with ϕ. The bulk drag coefficient decreases with the increase in stem Reynolds number in the range of Re = 65–685. Kothyari et al. (2009) measured directly the drag on a single cylinder within a staggered array of cylinders and found that the stem drag coefficient increases logarithmically with ϕ. The bulk drag coefficient slightly decreases with the increase in stem Reynolds number Re in the range of Re = 1000–5000. Cheng and Nguyen (2011) reported the similar trend and determined the C_d-Re relationship for cylinder arrays using a vegetated-related hydraulic radius as the characteristic length scale. Cheng (2013) applied the C_d-Re curve for an isolated cylinder to an array of cylinders using a generalized Reynolds number.

Most of the previous studies focused on rigid cylinders under uniform flow conditions. For emergent vegetation with high areal density, uniform flow condition seldom occurs and the flow will be gradually varied. Li and Tam (2002) have studied simulated semi-rigid vegetation (using black rubber rods) under gradually varied flow condition with gentle bed-slope of 1:1000. The longitudinal momentum equation was used to determine the mean bulk drag coefficient through the matching of the computed and measured water surface profiles. While the use of circular cylinders to simulate vegetation stems is common, some species of vegetation are of blade type. There is not much study of vegetated flows with blade type elements. Available works include Nezu and Sanjou (2008), Yang and Choi (2009). All these works focus on the flow and turbulent characteristics of the vegetation under submerged condition.

Previous works indicate that the bulk drag coefficient may not solely dependent on the solid volume fraction. The distribution pattern of the stems in the array will be important. The present study aims to investigate the interference effects among the vegetation stems through laboratory flume measurements of gradually varied flow through blade-type vegetation elements. The longitudinal and lateral spacing between adjacent vegetation elements are changed in different sets of experiments to identify the mechanism of flow interference. The bulk drag coefficient is determined based on the longitudinal momentum equation for gradually varied flow. An empirical formula relating C_d and the longitudinal and lateral stem spacing is proposed.

2. Wake interference effects of multiple stems

Vegetation of finite length and width commonly occurs along river channels. The flow is often nonuniform and the water surface profile is gradually varied. The key parameter to be determined is the bulk drag coefficient for each stem. The total drag consists of the shear force and the pressure drag, which is affected by the presence of multiple stems that alter the flow conditions.

The flow around a single stem will separate at certain location on the stem surface, creating a low pressure wake region behind the stem. The pressure difference between the windward and leeward surfaces generates the pressure drag. In addition, the flow will exert a viscous force on the stem surface and generates a shear friction drag on the stem. The total drag consists of the pressure drag and the friction drag. For bluff bodies including vegetation stem, the pressure drag is much larger than the friction drag.

In an array of stems, the phenomenon is complicated. If a stem is situated behind an adjacent stem, it will be subjected to a lower velocity of flow due to the blocking effect of the upstream stem. If it is located closely to the upstream stem, the wake behind the upstream stem will be interfered with the eddy scale limited by the stem spacing. The reduction in velocity and reduction in the eddy size will lower the pressure drag. The overall drag reduction effect is called the sheltering effect.

On the contrary, if a stem is situated close to an adjacent stem transversely, the width of the flow path will be narrowed. The velocity of flow in the narrow gap will be significantly increased due to the continuity requirement. A significant portion of the pressure energy will be converted into the kinetic energy, resulting in a further decrease of the pressure at the wake region behind the stem. The drag will then be increased due to the larger pressure difference across the stem. The overall drag increase effect is called the channeling effect.

Understanding the "*sheltering*" and "*channeling*" effects can be useful for river restoration. The former can be used as an erosion control mechanism and provide a favorable habitat for aquatic animals. The latter can enhance solute transport and reduce sediment accumulation. To strike a balance between the ecological preservation and hydraulic resistance reduction, vegetation management can take account the interference effects among individual stems.

3. Theory

The drag force on a piece of vegetation due to fluid flow can be expressed as

$$F_d = -\mu \iint_{S_c} \frac{\partial \vec{u}}{\partial n} dS + \iint_{S_c} p \cdot \vec{n} dS \tag{1}$$

Where μ ($N\ s/m^2$) is the viscosity, $\vec{u}$ *(m/s)* is the velocity vector at the vegetation surface, $\vec{n}$ is the outward unit normal vector on S_c, S_c (m^2) denotes all surfaces, p (N/m^2) is the pressure. On the right hand size of Eq. (1), the first term represents the viscous shear force and the second term represents the pressure force due to the wake. In general, the viscous shear force is small and a nondimensional drag coefficient is used to characterize the drag force as follows:

$$C_{d1} = \frac{F_d}{0.5\rho A_p U^2} \tag{2}$$

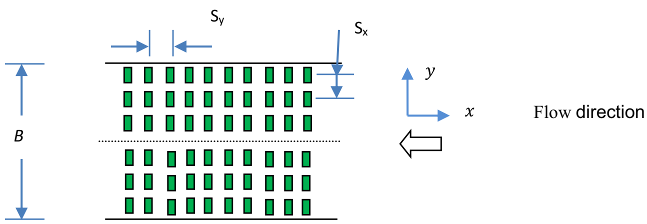

Fig. 1. Layout of vegetation elements.

Fig. 2. A sectional plan view of the dense vegetation ($\phi = 0.1214$ array).

where ρ *(kg/m³)* is the fluid density, A_p (m^2) is the projected area, and U (*m/s*) is the average pore velocity approaching the vegetation. For emergent stem-type vegetation, $A_p = hb_v$, where h (*m*) is the water depth and b_v (*m*) is the width of stem. For vegetation with high areal density and fully occupied a channel, the average pore velocity is given by

$$U = \frac{Q}{Bh(1-\phi l^*)} \tag{3}$$

where Q (m^3/s) is the discharge of the channel, B (*m*) is the channel width, $l^* = h_v / h$ is the ratio of wetted length of stem to flow depth, and $l^* = 1$ for emergent condition. In the present, work the blade-type stems are deployed with a regular rectilinear grid pattern shown in Fig. 1. The solid volume fraction of vegetation is defined by $\phi = {b_v t_v}\big/{S_x S_y} = Nb_v t_v = \lambda t_v$ (-), where t_v (*m*) is the thickness of the stem, N ($1/m^2$) is the number of vegetation stems per unit area, and S_x (S_y) in (*m*) is the lateral (longitudinal) center-to-center spacing between stems as defined in Fig. 1. The frontal area of vegetation per unit volume (areal density) is then given by $\lambda = \frac{b_v}{S_x S_y} = Nb_v$ (m^{-1}).

Under a gradually varied flow condition, the drag force F_D, water depth h and velocity U will vary with location. To account for the mean bulk drag characteristics of the vegetation canopy, a spatially averaged bulk drag coefficient is defined as follows:

$$C_d = \frac{1}{L}\int_0^L \frac{F_D(x)}{0.5\rho h(x)\lambda[U(x)]^2}dx \tag{4}$$

The integral can be satisfied by setting

$$F_D = 0.5C_d\,\rho h\lambda U^2 \tag{5}$$

The longitudinal momentum equation for a control volume ($B\times\Delta x\times h$, where Δx (*m*) is the differential longitudinal length) can be given by

$$\rho\frac{\Delta U}{\Delta t} + \rho U\frac{\Delta U}{\Delta x} = -\rho g\frac{\Delta h}{\Delta x} - \tau_s + \rho g S - \frac{1}{2(1-\phi)}\rho C_d\lambda U^2 \tag{6}$$

where τ_s*(N/m²)* is the boundary shear stress, S (-) is the bed-slope, g (m/s^2) = acceleration due to gravity, and Δ denotes the differential change. The left hand side of the equation denotes the rate of change in momentum in the control volume. The first, second, third and fourth terms on the right hand side of the equation are pressure, viscous stress, gravity and vegetation drag, respectively.

Assuming steady flow condition, neglecting the shear forces at the bed and sidewalls, as well as utilizing the continuity equation $UhB(1-\phi) = Q$ = constant, we obtain

$$\left(g - \frac{U^2}{h}\right)\frac{\Delta h}{\Delta x} = gS - \frac{1}{2(1-\phi)}C_d\lambda U^2 \tag{7}$$

Integrating Eq. (7) between the limits of the initial flow depth, h_o to h with respect to distance x gives the following expression:

$$F(h) = \int_{h_o}^{h}\left(\frac{g - \frac{U^2}{h}}{gS - \frac{1}{2(1-\phi)}C_d\lambda U^2}\right)dh = x + \text{constant} \tag{8}$$

From the measured water surface profile (h against x) for different flow cases, $F(h)$ in Eq. (8) can be evaluated numerically by assuming a value of the bulk drag coefficient for the entire canopy. Using the trial and errors method, the mean value of C_d can be obtained by fitting a straight line of unit slope for the plot of $F(h)$ against x.

The above equation is well applied for flow through dense vegetation (e.g., Fig. 2). The hydraulic resistance force offered by the vegetation is very high and exceeds the gravitational force provided by the bed slope. A water surface profile will be developed to provide the required gravitational force and a gradually varied flow condition is resulted.

4. Experiments

The experiments have been conducted in a 0.31 m wide, 0.40 m deep and 12.50 m long tilting and slope-adjustable rectangular flume. The sidewalls and bottom are made of glass and steel, respectively. Flow rates are measured by an electromagnetic flowmeter installed in the flow return pipe. The flow at the entrance of the channel is straightened using a series of honeycombs, thereby preventing the formation of large-scale flow disturbances. The flume receives a constant supply of water from a head tank with adjustable tailgate at the downstream end of the flume to regulate the flow depth. Water leaving the flume enters a large sump under the flume, where it is re-circulated to the constant head tank with a pump. Two wheeled trolleys, which can be moved along the double-rail track on the top of the flume, are used to mount the Vernier point gauge with ±0.5 mm accuracy. The longitudinal water surface profile is measured by the point gauge moving along the channel.

Table 1
Experimental conditions and measured C_d, fixed lateral spacing.

S_x(m) = 0.0125	Q (m^3/hr) =	5	10	15	20	25	30
S_y(m) = 0.0083	Re =	627	745	853	917	973	1008
λ(1/m) = 72.9	C_d =	2.0	2.2	2.3	2.4	2.5	2.2
	U (m/s)	0.083	0.099	0.113	0.122	0.129	0.134
	Fr =	0.107	0.099	0.098	0.095	0.093	0.089
S_y(m) = 0.0125	Re =	507	605	685	744		
λ(1/m) = 48.2	C_d =	3.3	3.2	3.2	3.1		
	U (m/s)	0.067	0.080	0.091	0.099		
	Fr=	0.080	0.074	0.072	0.071		
S_y(m) = 0.025	Re =	515	630	719	798		
λ(1/m) = 24.1	C_d =	6.0	5.7	5.2	4.8		
	U (m/s)	0.068	0.084	0.096	0.106		
	Fr =	0.084	0.080	0.079	0.081		
S_y(m) = 0.05	Re =	694	769	865	945	1040	
λ(1/m) = 12.0	C_d =	6.8	6.9	6.8	6.0	5.2	
	U (m/s)	0.092	0.102	0.115	0.126	0.138	
	Fr =	0.132	0.109	0.106	0.105	0.108	
S_y(m) = 0.1	Re =	703	884	1015	1083	1215	
λ(1/m) = 6.0	C_d =	10.4	9.2	8.1	7.8	6.5	
	U (m/s)	0.093	0.117	0.135	0.144	0.161	
	Fr =	0.135	0.135	0.136	0.130	0.138	

The vegetation patch is of length 2.4m and width 0.3 m, which is simulated with arrays of semi-rigid cable tile blades. The cable tile blades are of 0.25m height, 0.00753m width and thickness of 0.00168 m and were fixed on a PVC board (Fig. 2). The board is placed into the flume with the bed-slope fixed at 1.67%. Two sets of experiments are purposely chosen. One set is with S_x kept constant and S_y varying. The other set is with S_y kept constant and S_x varying. A total of 55 experimental runs have been conducted, with a maximum of six flow rates used in each array pattern. For each experiment, the flow depth has been measured at 5 cm interval along the vegetation patch length. The average pore velocity has been calculated from the measured flow rate using Eq. (2). For the cases with S_y kept constant and λ greater 9m^{-1}, the water level was very low due to the high flow velocity, and strong surface waves were observed. In order to minimize the uncertainty in the measurement, the minimum flow rate was set at $15m^3/h$. Details about S_x, S_y, λ, Q and stem Reynolds number Re and Froude number Fr for each experiment are shown in Table 1 and Table 2, where $\mathrm{Re} = Ub_v/\upsilon$, υ = kinematic viscosity and $\mathrm{Fr} = U/\sqrt{(gh_0)}$.

Table 2
Experimental conditions and measured C_d, fixed longitudinal spacing.

S_y(m) = 0.02	Q (m^3/hr) =	5	10	15	20	25	30	35
S_x(m) = 0.02	Re =	593	761	871	948	1037		
λ(1/m) = 18.8	C_d =	3.0	2.9	2.8	2.8	2.7		
	U (m/s)	0.076	0.098	0.112	0.122	0.133		
	Fr =	0.101	0.103	0.103	0.102	0.104		
S_x(m) = 0.025	Re =	607	744	865	975	1055	1141	
λ(1/m) = 15.1	C_d =	3.6	3.8	3.6	3.3	3.2	3.0	
	U (m/s)	0.077	0.096	0.112	0.126	0.137	0.148	
	Fr =	0.105	0.101	0.103	0.107	0.108	0.111	
S_x(m) = 0.04	Re =			1270	1414	1530	1632	1726
λ(1/m) = 9.4	C_d =			2.0	1.9	1.9	1.8	1.8
	U (m/s)			0.166	0.185	0.200	0.213	0.226
	Fr =			0.186	0.189	0.191	0.192	0.193
S_x(m) = 0.05	Re =			1385	1514	1627	1737	1826
λ(1/m) = 7.5	C_d =			1.8	1.7	1.7	1.7	1.7
	U (m/s)			0.182	0.199	0.213	0.228	0.239
	Fr =			0.213	0.211	0.210	0.212	0.211
S_x(m) = 0.08	Re =			1594	1838	1910	2040	2125
λ(1/m) = 4.7	C_d =			1.5	1.5	1.5	1.4	1.4
	U (m/s)			0.210	0.242	0.252	0.269	0.280
	Fr =			0.265	0.284	0.269	0.271	0.267
S_x(m) = 0.1	Re =			1886	2122	2263	2397	2583
λ(1/m) = 3.8	C_d =			1.2	1.2	1.2	1.1	1.1
	U (m/s)			0.249	0.280	0.299	0.316	0.341
	Fr =			0.342	0.353	0.348	0.346	0.359

5. Results and discussion

The results of some measured water surface profiles for different values of λ and flow rates are shown in Fig. 3a. For most cases, the water depth slightly decreases in the direction of flow. This shows that the resistance force offered by the vegetation is greater than the gravitational force component parallel to the channel bed. Water flow is retarded and a water surface slope steeper than the bottom slope is produced to balance the resistance force generated by vegetation. The computed water

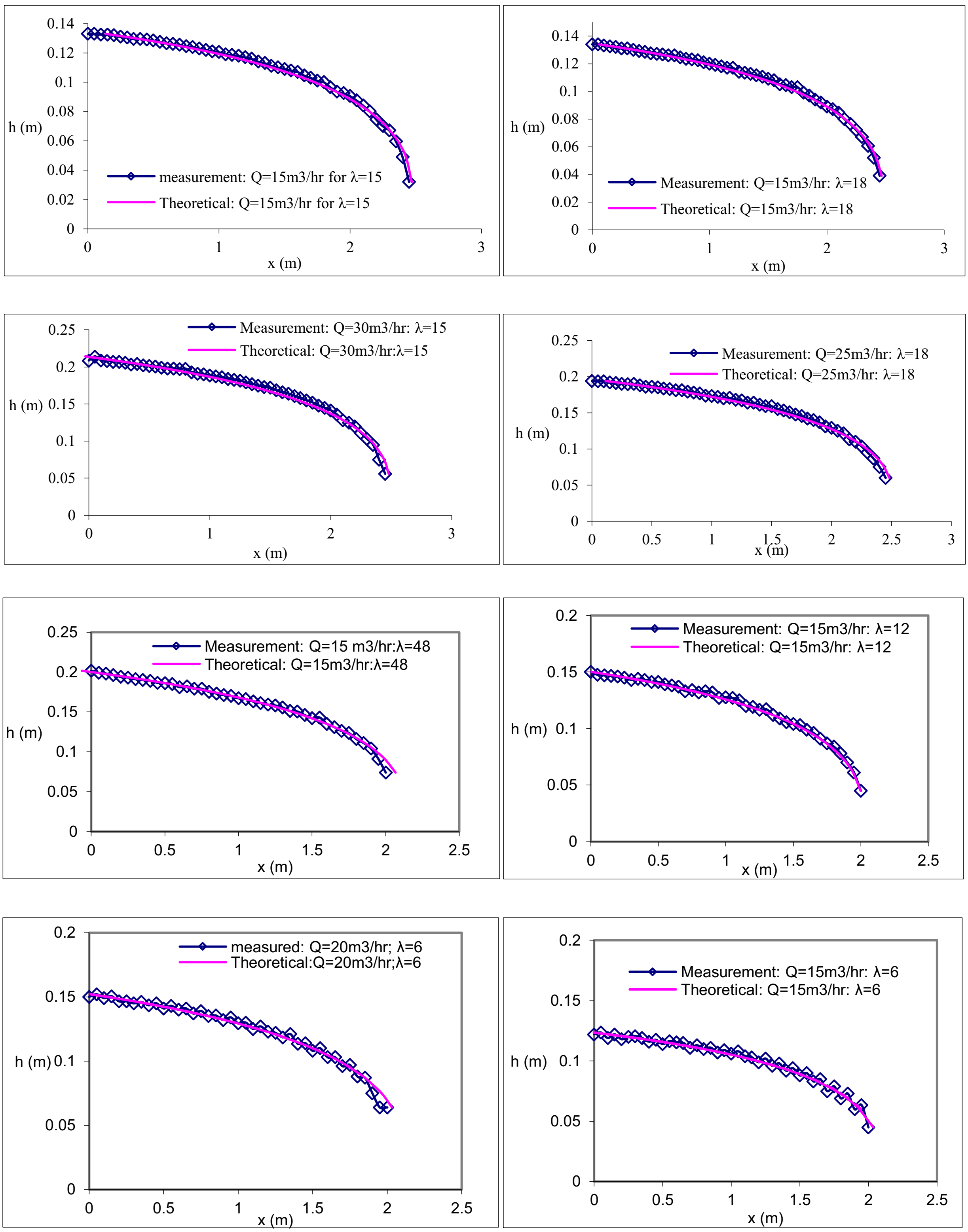

Fig. 3. Water surface profiles for flow through vegetation.

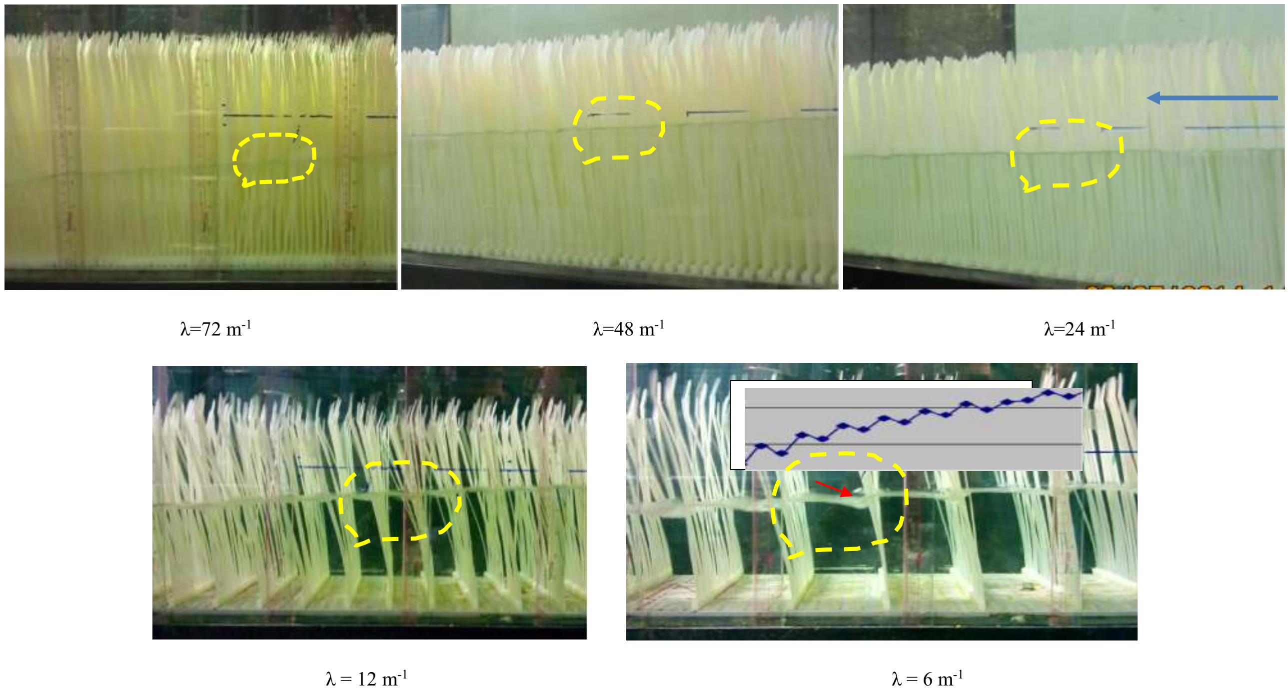

Fig. 4. Snapshots of flow through simulated vegetation with constant S_x.

surface profiles using best-fit value of C_d are included in Fig. 3a. The good agreement between the measured and semi-theoretical results shows the validity of Eq. (6) and a high reliability of the estimated C_d value. Generally, the water level increases with increase in λ under the same flow rate. The estimated C_d for all cases are tabulated in Table 1 and Table 2. During the experiments, it was observed that the vegetation elements were slightly deflected. As the elements were emergent and the deflection was small, the effect of the leaning of the elements on the drag coefficient is considered negligible. The water level measurement interval of 5 cm is sufficiently fine. Sensitivity analysis has been carried out by determining C_d using water level data at 10 cm interval, and the difference between the two set of results is within a few percent.

For cases with smaller S_x and larger S_y, the channeling effect is apparent. Fig. 4 shows that there is a significant pressure drop (water level drop) for the flow through the constriction between two adjacent blades for the case $\lambda = 6\text{m}^{-1}$ ($S_x = 0.0125$m, $S_y = 0.1$m) highlighted in the yellow dashed circles. At the downstream region of the stems, the velocity decreases due to the shear action. This is similar to the spreading of a water jet. Part of the kinetic energy is converted back to the pressure energy when the flow strikes against the downstream blades and an increase in water level is resulted. The process is repeated when the flow encounters another lateral row of blades downstream. Consequently, the water level displays a staircase type of profile. When S_y is reduced, the jet spreading effect is not so significant due to the blocking effect of the downstream blades. The velocity in the channel region formed by two adjacent longitudinal rows of blades remains high, and there is not so much flow strikes against the blades. The pressure drop across the blades is thus smaller and the water surface profile is smoother (Fig. 4, $\lambda = 72\text{m}^{-1}$, 48m^{-1}, 24m^{-1}).

To estimate the energy loss of the flow through a transverse row of stems with narrow openings, an analogy with the orifice flow can be made. The relationship between the drag coefficient C_d and the discharge coefficient C_0, the coefficient of velocity C_v, and the geometric dimensions of the stems has been derived and shown in Appendix. Using the typical values of the C_0 and C_v, the estimated C_d is high and matches the measured value. Fig. 5 shows that the drag coefficient, C_d decreases with increasing stem Reynolds number for the range $500 < \text{Re} < 1500$. The drag coefficient exhibits more or less a linear dependence on the stem Reynolds number. Similar trend had been observed for cylinder arrays of similar range of Re (Cheng and Nguyen, 2011; Tanino and Nepf, 2008). For the set of experiments with S_x fixed, C_d is insensitive to the variation of Re for cases with higher value of λ (Fig. 5a). For the set of experiments with S_y fixed, C_d is insensitive to the variation of Re for cases with lower value of λ and higher velocity (Fig. 5b).

The experimental results indicates that for cases with S_x fixed, at a smaller value of S_y, the change in velocity will not alter the flow pattern since the wake region is limited by the longitudinal spacing of adjacent blades S_y. The resulting C_d is approximately a constant. For a larger value of S_y, the flow pattern is affected by the magnitude of the velocity and a decreasing trend of C_d with Re is resulted. For cases with S_y fixed, at a larger value of S_x, the lateral spacing between adjacent blades is sufficiently wide, and the flow pattern is not affected by the variation in velocity. When S_x is small, the interference effect between two laterally adjacent blades becomes strong and is affected by the magnitude of the velocity.

Fig. 6a shows that C_d decreases with increasing areal density of vegetation when the transverse spacing S_x is fixed. In this set of experiments, the speed up ratio of the flow through the contracting path between two transversely adjacent blades is

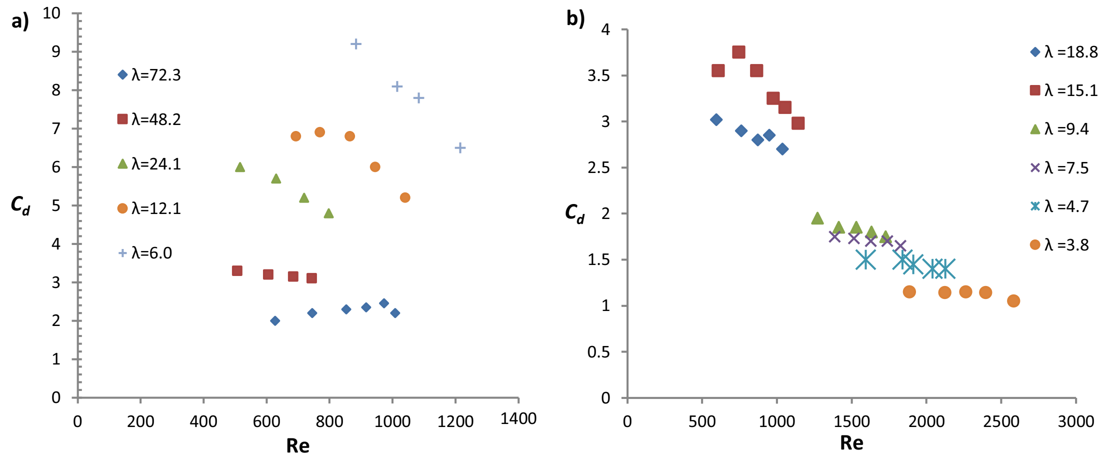

Fig. 5. Bulk drag coefficient as a function of stem Reynolds number for cases of different areal density of stems λ: a) S_x constant; b) S_y constant.

more or less unchanged since S_x is a constant. The decrease of S_y increases the effect of wake interference induced by the blades, resulting in a lower drag (sheltering effect). Fig. 6b shows that C_d increases with increasing areal density of vegetation when the longitudinal spacing S_y is fixed. In this set of experiments, the wake interference (sheltering) effect is more not less unchanged. The decrease in S_x increases the speed up ratio of the flow through the contracting path in between two transversely adjacent blades, resulting in a higher drag (channeling effect). The increasing trend in Fig. 6b is confirmed from the interpolated value in Fig. 6a. For the case of $S_x = 0.0125$m and $S_y = 0.02$m, $\lambda = 30.1$/m, the interpolated value in Fig. 6a gives C_d ~5.

To investigate the contribution of the viscous force and pressure force to the total drag force, the nondimensional drag $f_d = F_d/(\mu U)$ is plotted against Re. Ergun (1952) proposed an equation for drag force in packed columns of the following form:

$$f_d = a_0 + a_1 \mathrm{Re} \tag{9}$$

where a_0 represents the contribution of the viscous shear stress on the stem surface, and a_1 represents the contribution of the pressure drop in the stem wake.

Fig. 7 illustrates the normalized drag force f_d as a function of Re. For cases with S_x kept constant, f_d varies approximately linearly with Re for cases with small S_y. For a given Re, f_d increases with decreasing λ, showing that the channeling effect plays a dominant role. For cases with larger S_y, the relationship between f_d and Re deviates from a straight line. If the data are fitted by a straight line, the intercept will give a high value. As the viscous force cannot be so large, the high value of a_0 is expected to be caused by the jetting and vortex shedding mechanisms. It is likely the best-fit line of the data for cases with large S_y will be a curve bending toward the origin at low Reynolds number. Based on the straight-line fitting, it is found that a_0 increases with S_y (Fig. 8), indicating that the effects of vortex shedding and jet spreading are more important for larger S_y. The negative value of a_0 at small S_y is probably due to the uncertainty in data fitting. A slight change in the slope of the straight line will easily generate a negative intercept. The coefficient a_1 decreases with increase of S_y showing that the pressure loss ratio due to kinetic energy dissipation decreases with the longitudinal spacing.

For the cases with S_y kept constant, f_d generally varies linearly with Re. For a given Re, f_d increases with increasing λ, showing that the sheltering effect plays a dominant role. The

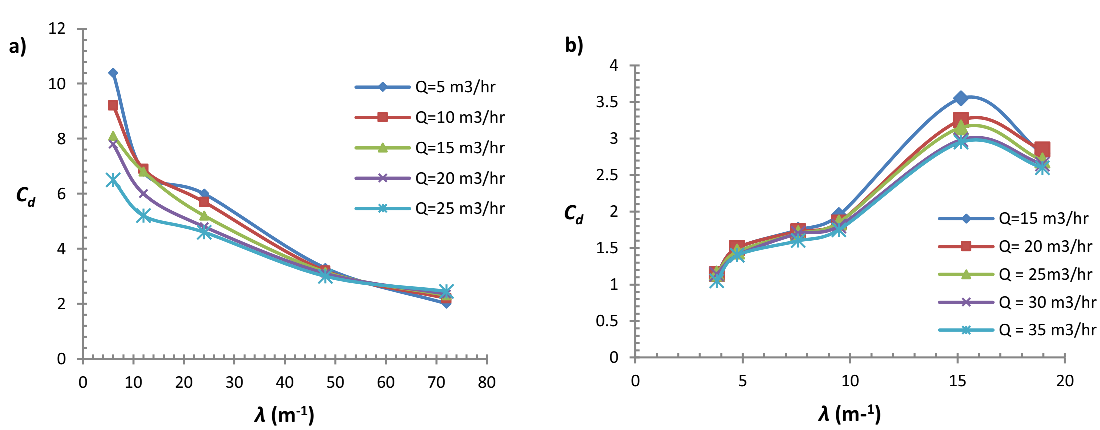

Fig. 6. Bulk drag coefficient as a function of areal density of vegetation: a) S_x constant; b) S_y constant.

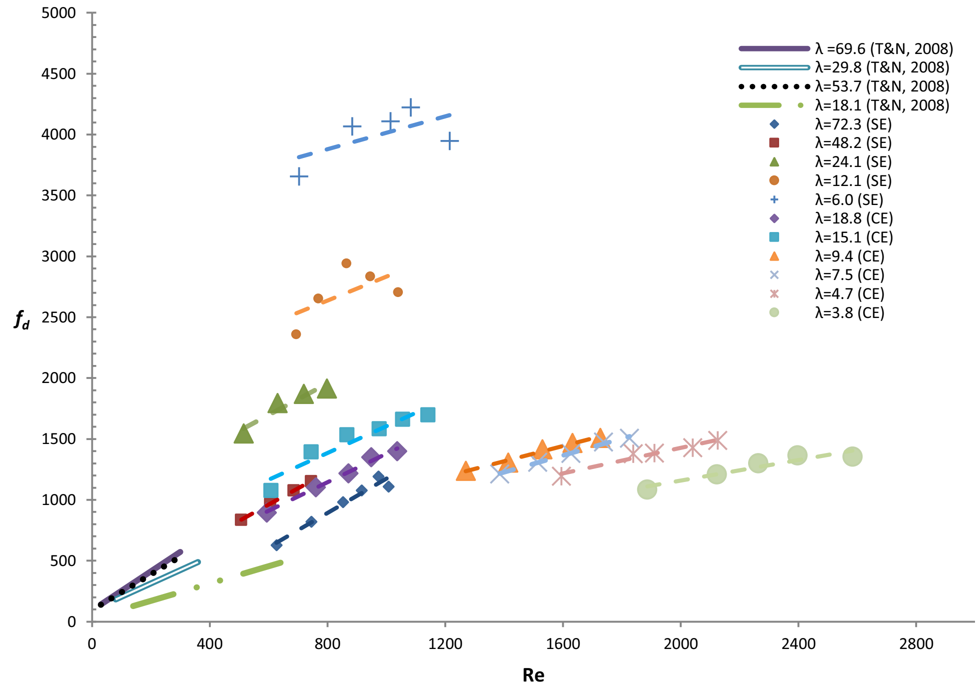

Fig. 7. Normalized drag force as a function of Reynolds number (SE refers to sheltering effect, S_x = constant and CE refers to channeling effect, S_y = constant).

results are similar and consistent with those obtained by Tanino and Nepf (2008) for closely packed cylinders in the Reynolds number range of 25–685 (Fig. 7). The intercept a_0 scatters around a mean value of 350 (Fig. 8), indicating the contribution of the viscous drag and other mechanisms does not vary significantly with S_x. The slope a_1 decreases with the increase in S_x, showing that the pressure drop ratio decreases with the increase of lateral spacing. This is due to that the wider the lateral spacing, the lesser the flow contraction will be.

The variation of normalized drag with Froude number Fr is shown in Fig. 9. The range of variation of Froude number for each case is narrow, generally within 20% from the mean value. For the cases with $S_x = 0.0125$m, the normalized drag appears to decrease with the increase in Fr. The uncertainty can be high as the range of Froude number is narrow. For cases with $S_y = 0.02$m, the normalized drag appears to be independent of Fr. Therefore, it can be concluded that the normalized drag is insensitive to Fr in the range of experimental conditions tested.

6. Fitting equation

It is known that for an isolated 2D plate under a high Reynolds number flow, the drag coefficient is $C_d = 2$ (e.g., Hoerner, 1965). In this study, we have obtained experimental results for drag coefficient of multiple plates in the Reynolds number range 500–2600, with different longitudinal spacing or lateral spacing. To fit the data, an asymptotic value $C_{d0} = 2$ is adopted. The fitting equation is proposed of the following form:

$$C_d = C_{d0}\{f(S_y)\}\{g(S_x)\} \tag{10}$$

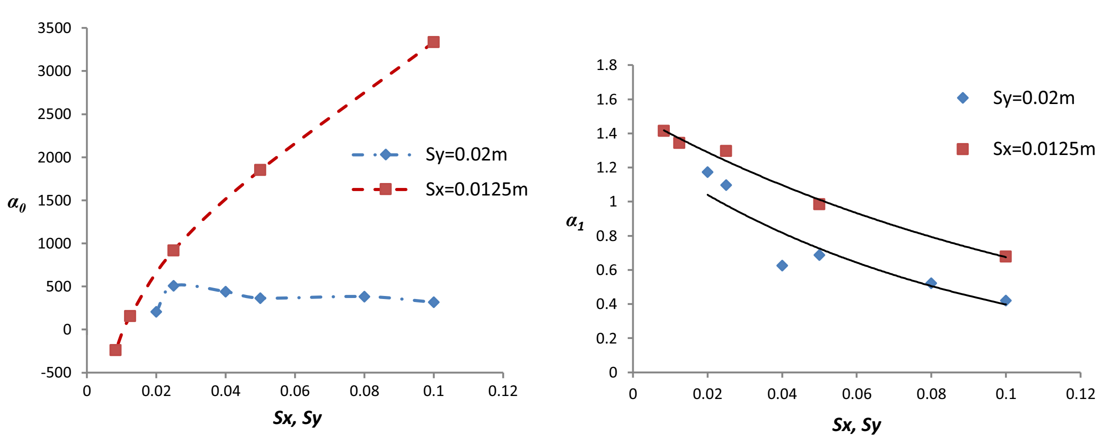

Fig. 8. Dependency of a_0 and a_1 on lateral (S_x) and longitudinal spacing (S_y).

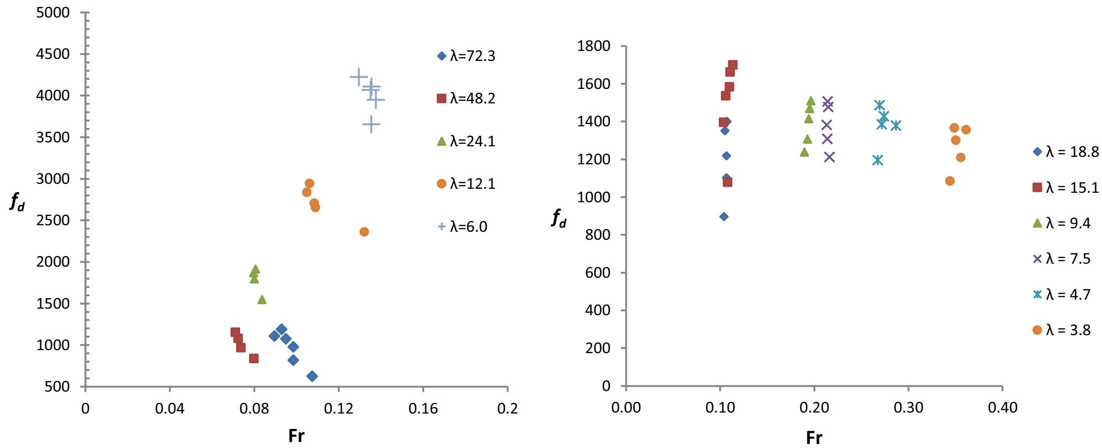

Fig. 9. Effect of normalized drag force on Froude number.

$$f(S_y)=\left\{1-\beta e^{-K\left(\frac{S_y}{b_v}\right)}\cdot Re^{-\gamma}F_r^{-\vartheta 1}\right\}$$

$$g(S_x)=\left\{1+\alpha e^{-L\left(\frac{S_x}{b_v}\right)}\cdot Re^{-\delta}F_r^{-\vartheta 2}\right\}$$

For $S_x\to\infty$; $S_y\to\infty$ and $R_e\to\infty$, $C_d\to C_{d0}=2$.

Using the multiple regression method, a good match between the fitting equation and the data is obtained (Fig. 10) with the parameters taking the following values: $\beta=2.4831$; $\alpha=2830$; $K=0.1256$; $L=0.1223$; $\gamma=0.1490$; $\delta=0.9288$; $\vartheta_1=0.0150$; $\vartheta_2=0.0350$. Fig. 10 shows the fitting results, the mean absolute error of the fitting is 9.5%. The results show that the effect of Fr on C_d is not significant for subcritical flows, as reflected in the small values of the exponents ϑ_1 and ϑ_2. This has been pointed out in the previous studies (e.g., Kothyari et al., 2009).

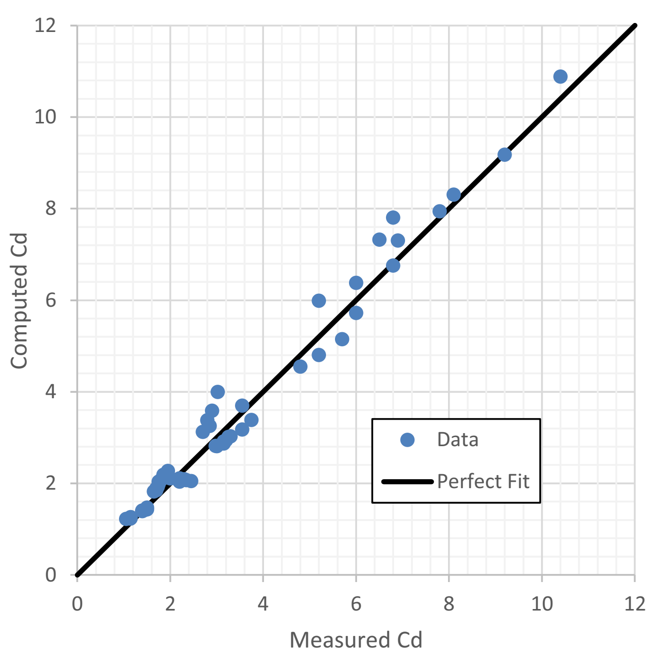

Fig. 10. Fitting results of C_d using equation 10.

Based on the fitting equation, it can be demonstrated that the relationship between C_d and ϕ for a fixed Reynolds number is not unique. By fixing S_x and varying S_y, C_d decreases with increasing ϕ. By fixing S_y and varying S_x, C_d increases with ϕ. Fig. 11 shows the decreasing trend for $S_x=0.0125$m, and increasing trend for $S_y=0.02$m. The Reynolds number for both cases is fixed at 1000. The observation helps to explain the previous contradictory results that the drag coefficient increases with ϕ (Kothyari et al., 2009; Tanino and Nepf, 2008), and the drag coefficient decreases with ϕ (Nepf, 1999). The distribution pattern of the individual stems plays a significant role. Similar trends are observed for normalized drag f_d as f_d is governed by C_d at large Re.

It is noted that the value of C_d is quite large for small S_x and large S_y. The drag in this case is governed by the channeling effect. The transverse gap between the plates is narrow and the velocity of flow through the gap is increased significantly. Comparing to the case with wide gap, more pressure energy is converted into the kinetic energy and the pressure behind the

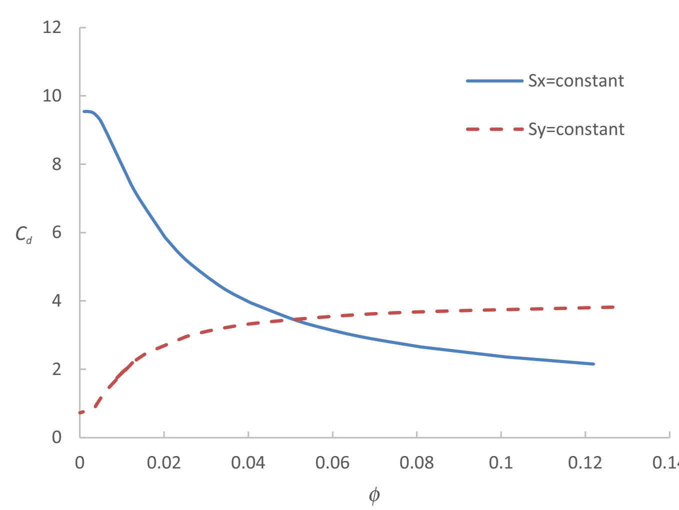

Fig. 11. Non-unique relation between C_d and ϕ.

plate is further reduced, resulting in a large drag. The largest drag coefficient computed from the experimental data is about 9, over four times larger than that of an isolated plate. This is consistent with the previous works. For example, Tanino and Nepf (2008) found that the drag in a random array of circular cylinders can be three or four times larger than that of an isolated circular cylinder.

7. Conclusions

Laboratory experiments were conducted to investigate the hydraulic behavior of semi-rigid blade type vegetation under subcritical gradually varied flow conditions. The longitudinal momentum equation relating the vegetation resistant force and water surface slope has been used to estimate the mean bulk drag coefficient C_d. The results show that C_d decreases with increasing Re, is not dependent uniquely on the solid volume fraction but depends on the distribution pattern of the vegetation elements. By decreasing the transverse spacing S_x and keeping S_y constant, C_d increases with increasing solid volume fraction due to the channeling effect. By increasing the longitudinal spacing S_y and keeping S_x constant, C_d decreases with increasing solid volume fraction due to the sheltering effect. The inertial contribution due to pressure loss in the stem wake increases with the decrease in transverse spacing, while the effects of viscous shear stress, vortex shedding and jet spreading effects increases with the increase in longitudinal spacing over the experimental range. An empirical equation is proposed for the calculation of the mean bulk drag coefficient.

Acknowledgement

This work is supported by the Research Grant Council of the Hong Kong Special Administrative Region under Grant No. 5200/12E and a grant from the Hong Kong Polytechnic University.

Appendix

For flow through a transverse row of stems, the streamlines will be contracted at the openings bounded by adjacent stems. If the flow is relatively undistributed by the upstream and downstream blades, and the transverse spacing is similar to the width of blade, the orifice flow equation can be used.

The flow scenario is shown in Fig. A1. The flow rate through an opening can be computed by the orifice flow equation as follows:

$$Q = C_0 A_0 \sqrt{\frac{2(P_1 - P_c)}{\rho\left(1 - \frac{A_0^2}{A_1^2}\right)}} \quad \text{(A.1)}$$

Where C_0 is the discharge coefficient accounting for the flow contraction and head loss; P_1 and P_c are the pressure at section 1 and section c, respectively; A_0 is the area of opening; A_1 is the upstream sectional area of the control volume at section 1.

The discharge through the opening is given by

$$Q = V_1 A_1 = C_0 A_0 V_{ideal} \quad \text{(A.2)}$$

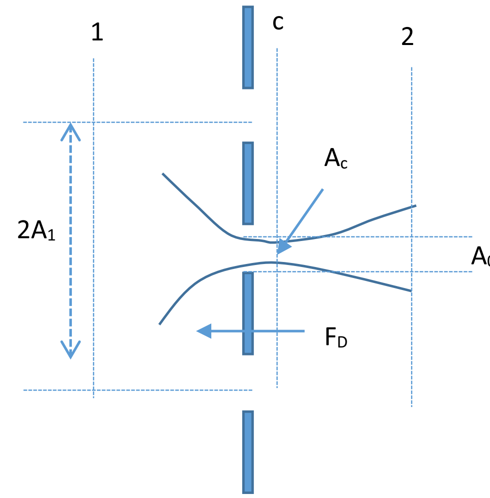

Fig. A1. Schematic diagram of flow though a row of plates.

where V_{ideal} is the idealized velocity at section c if there is no flow contraction and no energy loss. Applying the momentum equation from section 1 to section c, we obtain

$$F_D = (P_1 - P_c)A_1 - \rho Q(V_c - V_1)$$

Where F_D is the resistance force offering by a stem, V_1 is the velocity at section 1, V_c is the velocity at the vena contracta and is given by

$$V_c = C_v V_{ideal} \quad \text{(A.3)}$$

Where C_v is the coefficient of velocity. The drag coefficient C_d is defined by

$$C_D = \frac{F_D}{\frac{1}{2}\rho(A_1 - A_0)V_1^2} \quad \text{(A.4)}$$

Hence

$$C_D = \left(\frac{A_1^2}{C_0^2 A_0^2} - \frac{1}{C_0^2} - 2\frac{C_v A_1}{C_0 A_0} + 2\right) \Bigg/ \left(1 - \frac{A_0}{A_1}\right) \quad \text{(A.5)}$$

As an example, if $C_0 = 0.7$, $C_v = 1$, $A_1 = 0.0125$m, $A_0 = 0.0050$m, the above equation gives $C_D = 9.4$.

References

Armanini, A., Righetti, M., Grisenti, P., 2005. Direct measurement of vegetation resistance in prototype scale. J. Hydraul. Res. 43 (5), 481–487.

Busari, A.O., Li, C.W., 2014. A hydraulic roughness model for submerged flexible vegetation with uncertainty estimation. J. Hydro Environ. Res. 9 2 268–280

Cheng, N.S., 2013. Calculation of drag coefficient for arrays of emergent circular cylinders with pseudofluid model. J. Hydraul. Eng. 139 (6), 602–611.

Cheng, N.S., Nguyen, H.T., 2011. Hydraulic radius for evaluating resistance induced by simulated unsubmerged vegetation in open-channel flows. J. Hydraul. Eng. 137 (9), 995–1004.

Ergun, S., 1952. Fluid flow through packed columns. Chem. Eng. Prog. 48 (2), 89–94.

Fathi-Moghadam, M., Kouwen, N., 1997. Nonrigid, nonsubmerged vegetative roughness on floodplains. J. Hydraul. Eng. 123 (1), 51–57.

Hoerner, S.F., 1965. Fluid Dynamic Drag. Published by the author, Bakersfield, CA.

James, C.S., Birkhead, A.L., Jordanova, A.A., O'Sullivan, J.J., 2004. Flow resistance of unsubmerged vegetation. J. Hydraul. Res. 42 (4), 390–398.

Kays, W., London, A., 1955. Compact Heat Exchangers. Natl. Press, Palo Alto, CA.

Kothyari, U.C., Hayashi, K., Hashimoto, H., 2009. Drag coefficient of unsubmerged rigid vegetation stems in open channel flows. J. Hydraul. Res. 47 (6), 691–699.

Kouwen, N., Fathi-Moghadam, M., 2000. Friction factors for coniferous trees along rivers. J. Hydraul. Eng. 126 (10), 732–740.

Li, C.W., Tam, Y.F., 2002. Gradually varied flow through semi-rigid vegetation. In: The Proceedings of the 14th Congress of International Association of Hydraulic Engineering and Research (IAHR), Hong Kong, 15–18 December, 2004. pp. 859–864.

Li, C.W., Xie, J.F., 2011. Numerical modelling of free surface flow over submerged and highly flexible vegetation. Adv. Water Resour. 34 (4), 468–477.

Nepf, H.M., 1999. Drag, turbulence, and diffusion in flow through unsubmerged vegetation. J. Water Resour. 35 (2), 479–489.

Nezu, I., Sanjou, M., 2008. Turburence structure and coherent motion in vegetated canopy open-channel flows. J. Hydro Environ. Res. 62–90.

Nikora, V., Scott, L., Nina, N., Koustuv, D., Glenn, C., Michael, R., 2008. Hydraulic resistance due to aquatic vegetation in small streams: field study. J. Hydraul. Eng. 134 (9), 1326–1332.

Righetti, M., Armanini, A., 2002. Flow resistance in open channel flows with sparsely distributed bushes. J. Hydrol. (Amst.) 269, 55–64.

Stone, B.M., Shen, H.T., 2002. Hydraulic resistance of flow in channels with cylindrical roughness. J. Hydraul. Eng. 128 (5), 500–506.

Tanino, Y., Nepf, H., 2008. Laboratory investigation of mean drag in a random array of rigid, unsubmerged cylinders. J. Hydraul. Eng. 134 (1), 34–41.

Wu, F.C., Shen, H.W., Chou, Y.J., 1999. Variation of roughness coefficients for unsubmerged and submerged vegetation. J. Hydraul. Eng. 125 (9), 934–942.

Yang, W., Choi, S.U., 2009. Impact of stem flexibility on mean flow and turbulence structure in depth-limited open channel flows with submerged vegetation. J. Hydraul. Res. 47 (4), 445–454.

Zdravkovich, M., 1993. Interstitial flow field and fluid forces. In: Au-Yang, M.K. (Ed.), Technology for the '90's. Am. Soc. of Mech. Eng., New York, p. 634.

Zeng, C., Li, C.W., 2014. Measurements and modeling of open-channel flows with finite semi-rigid vegetation patches. J. Environ. Fluid Mech. 14, 113–134.